2

Numerical Modeling and Experimentation on Evaporator Coils for Refrigeration in Dry and Frosting Operational Conditions

Zine Aidoun, Mohamed Ouzzane and Adlane Bendaoud
CanmetENERGY-Varennes Natural Resources Canada
Canada

1. Introduction

The drive to improve energy efficiency in refrigeration and heat pump systems necessarily leads to a continuous reassessment of the current heat transfer surface design and analysis techniques. The process of heat exchange between two fluids at different temperatures, separated by a solid wall occurs in many engineering applications and heat exchangers are the devices used to implement this operation. If improved heat exchanger designs are used as evaporators and condensers in refrigerators and heat pumps, these can considerably benefit from improved cycle efficiency. Air coolers or coils are heat exchangers applied extensively in cold stores, the food industry and air conditioning as evaporators. In these devices, heat transfer enhancement is used to achieve high heat transfer coefficients in small volumes, and extended surfaces or fins, classified as a passive method, are the most frequently encountered. Almost all forced convection air coolers use finned tubes. Coils have in this way become established as the heat transfer workhorse of the refrigeration industry, because of their high area density, their relatively low cost, and the excellent thermo physical properties of copper and aluminum, which are their principal construction materials. Compact coils are needed to facilitate the repackaging of a number of types of air conditioning and refrigeration equipment: a reduced volume effectively enables a new approach to be made to the modular design and a route towards improving performance and size is through appropriate selection of refrigerants, heat transfer enhancement of primary and secondary surfaces through advanced fin design and circuit configurations. Circuiting, although practically used on an empirical basis, has not yet received sufficient attention despite its potential for performance improvement, flow and heat transfer distribution, cost and operational efficiency. In the specific case of refrigeration and air conditioning, a confined phase changing refrigerant exchanges heat in evaporators with the cold room, giving up its heat. The design and operation of refrigeration coils is adapted to these particular conditions. Geometrically they generally consist of copper tubing to which aluminum fins are attached to increase their external surface area over which air is flowing, in order to compensate for this latter poor convection heat transfer. Coils generally achieve relatively high heat transfer area per unit volume by having dense arrays of finned tubes and the fins are generally corrugated or occasionally louvered plates with variable spacing and number of passes. Internal heat transfer of phase changing refrigerant is high and varies

with flow regimes occurring along the tube passes. Flow on the secondary surfaces (outside of tubes and fins) in cooling, refrigeration or deep freezing, becomes rapidly complicated by the mass transfer during the commonly occurring processes of condensation and frost deposition, depending on the air prevailing conditions. Overall, geometric and operational considerations make these components very complex to design and analyse theoretically.

2. Previous research highlights

An inherent characteristic of plate fin-and-tube heat exchangers being that air-side heat transfer coefficients are generally much lower than those on the refrigerant side, an effective route towards their performance improvement is through heat transfer enhancement. Substantial gains in terms of size and cost are then made, on heat exchangers and related units, during air dehumidification and frost formation. In the specific case of evaporators and condensers treated here, it is the primary and secondary surfaces arrangements or designs that are of importance i.e. fins and circuit designs. These arrangements are generally known as passive enhancement, implying no external energy input for their activation. Fins improve heat exchange with the airside stream and come in a variety of shapes. In evaporators and condensers, round tubes are most commonly encountered and fins attached on their outer side are either individually assembled, in a variety of geometries or in continuous sheets, flat, corrugated or louvered. For refrigeration, fins significantly alleviate the effect of airside resistance to heat transfer. Heat exchangers of this type are in the class of compact heat exchangers, characterized by area densities as high as 700 m^2/m^3. Heat transfer enhancement based on the use of extended surfaces and circuiting has received particular attention in our studies. By discussing some of the related current research in the context of work performed elsewhere, it is our hope that researchers and engineers active in the field will be able to identify new opportunities, likely to emerge in their own research. Our efforts are successfully articulated around experimentation with CO_2 as refrigerant for low temperature applications and novel modeling treatment of circuit design and frost deposition control.

2.1 Modeling

Modeling of refrigeration heat exchangers for design and performance prediction has been progressing during the last two decades or so in view of the reduced design and development costs it provides, as opposed to physical prototyping. Most models handle steady state, dry, wet or frosting operating conditions. They fall into two main approaches: zone-by-zone and incremental. Zone-by-zone models divide the heat exchanger into subcooled, two-phase and superheated regions which are considered as independent heat exchangers hooked in series. Incremental methods divide the heat exchanger in an arbitrary number of small elements. They can be adapted to perform calculations along the refrigerant flow path and conveniently handle circuiting effects, as well as fluid distributions. Several models of both types are available in the literature for design and simulation, with different degrees of sophistication. Only a representative sample of existing research on heat exchanger coils is reported here and the main features highlighted. (Domanski, 1991) proposed a tube–by-tube computation approach which he applied to study the effect of non-uniform air distribution on the performance of a plate-and-tube heat exchanger. Based on the same approach, (Bensafi et al., 1997) developed a general tool for

design and simulation of finned-tube heat exchangers for a limited number of pure and mixed refrigerants in evaporation or condensation. This model can handle circuiting but requires user intervention to fix mass flows in each circuit. Since hydrodynamic and thermal aspects are treated independently, this manual intervention may affect the final thermal results, thus limiting the application to only simple cases. (Corberan et al., 1998) developed a model of plate- finned tube evaporators and condensers, for refrigerant R134a. They then compared the predicting efficiency of a number of available correlations in the literature for heat transfer and friction factor coefficients. This model is limited to computing the refrigerant side conditions. (Liang et al., 1999) developed a distributed simulation model for coils which accounts for the refrigerant pressure drop along the coil and the partially or totally wet fin conditions on the air side. (Byun et al., 2007) conducted their study, based on the tube-by-tube method and EVSIM model due to (Domanski, 1989) in which they updated the correlations in order to suit their conditions. Performance analysis included different refrigerants, fin geometry and inner tube configuration. Other detailed models such as those of (Singh et al., 2008) and (Singh et al., 2009) respectively account for fin heat conduction and arbitrary fin sheet, encompassing variable tube location and size, variable pitches and several other interesting features. (Ouzzane&Aidoun, 2008), simulated the thermal behaviour of the wavy fins and coil heat exchangers, using refrigerant CO_2. The authors used a forward marching technique to solve their conservation equations by discretizing the quality of the refrigerant. The iterative process fixes the outlet refrigerant conditions and computes the inlet conditions which are then compared with the real conditions until convergence is achieved. This method requires manual adjustments during the iterative process and is therefore not well adapted to handle complex circuiting. Moreover, on the air side, mean inlet temperatures are used before each tube, resulting in up to 3.5 % capacity variation, depending on the coil depth. In an effort to address the weaknesses of the above mentioned procedure and extend its computational capabilities (Bendaoud et al., 2011) further developed a new distributed model simultaneously accounting for the thermal and hydrodynamic behaviour and handling complex geometries, dry, humid and frosting conditions. The equations describing these aspects are strongly coupled, and their decoupling is reached by using an original method of resolution. The heat exchanger may be subdivided into several elementary control volumes, allowing for detailed information in X, Y and Z directions. Among the features which are being recognized by the research community as having an important impact on plate fin-and-tube heat exchangers in the refrigeration context, are the following:

2.1.1 Circuiting

In many cases the heat exchanger performance enhancement process focuses on identifying refrigerant circuitry that provides maximum heat transfer rates for given environmental constraints. In fact, refrigerant circuitry may have a significant effect on capacity and operation. However, the numerous possible circuitry arrangements for a finned tube heat exchanger are a contributing factor to the complexity of its modeling and analysis. Designing maximized performance refrigerant circuitry may prove to be even more challenging for new refrigerants with no previous experience or design data available. It is perhaps one reason that only a limited amount of work has been devoted to advance research and development on theses yet important aspects. (Domanski's, 1991) tube-by-tube model was designed to handle simple circuits in counter-current configurations and (Elison

et al., 1981), also using the tube-by-tube method built a model for a specified circuitry on fin and tube condensers. The same approach was adopted by (Vardhan et al., 1998) to study simple circuited plate-fin-tube coils for cooling and dehumidification. The effectiveness-NTU method was used but information was provided neither on refrigerant heat transfer and pressure drop conditions, nor on the airside pressure losses. Later (Liang et al., 2000) and (Liang et al., 2001) performed two studies on refrigerant circuitry for finned tube condensers and dry evaporators respectively. The condenser model combined the flexibility of a distributed model to an exergy destruction analysis to evaluate performance. The same modeling approach was applied to cooling evaporators. Six coil configurations with different circuiting were compared. In both condensers and evaporators the authors reported that adequate circuiting could reduce the heat transfer area by approximately 5%. It is to be noted however that only simple circuiting could be conveniently handled and no account was taken of the airside pressure drop. In common to the reported approaches, the hydrodynamics of the problem was not detailed. Circuiting arrangements with several refrigerant inlets and junctions were not fully taken care of, so that the user must fix a mass flux of the refrigerant in each inlet and in the process, the thermal-hydrodynamic coupling is lost, affecting the results. (Liu et al., 2004) developed a steady state model based on the pass-by-pass approach, accounting for heat conduction between adjacent tubes and circuitry by means of a matrix that fixes the configuration. (Jiang et al., 2006) proposed CoilDesigner, in the form of easy-to-use software. It handles circuitry in a similar manner to Liu's model but uses a segment by segment computational approach in order to capture potential parameter variations occurring locally. Mean values of heat transfer coefficients on both air and refrigerant sides are then calculated. This approximation generally leads to important differences between numerical and experimental results. CoilDesigner does not provide air-side pressure losses which may be important in large refrigeration installations. Another interesting indexing technique for complex circuitry was proposed by (Kuo et al., 2006). It is based on a connectivity matrix similar to those used in (Liu et al., 2004) and (Jiang et al., 2006) but introduces additional indices to indicate the number of main flows, first and second level circuitry. The related model is of distributed type for cooling with dry and wet conditions. The details of the modeling procedure for the coupled thermal hydraulic system represented by the air and refrigerant sides are not provided.

2.1.2 Frosting

Frost forms on evaporator coil surfaces on which it grows when operating temperatures are below 0 ^{o}C and the air dew point temperature is above the coil surface temperature. It affects considerably the performance by reducing the refrigeration capacity and the system efficiency. This performance degradation occurs because frost is a porous medium composed of air and ice with poor thermal conductivity. The frost layer increases the air-refrigerant thermal resistance. Moreover, frost accumulation eventually narrows the flow channels formed by tubes and adjoining fins, imposing an increasingly higher resistance to air flow. This effect is marked at the leading edge, causing a rapid decline in heat transfer and early blockage of the channels at this location. Consequently, the rows of finned tubes located at the rear of multi-row coils may become severely underused. It is the authors' belief that circuiting can play a role to alleviate this effect by more uniformly distributing capacity and temperature among rows. Available theoretical literature on coil frosting is limited due to complex equipment geometries. Selected work is reported herein:

(Kondepudi et al., 1993a) developed an analytical model for finned-tube heat exchangers under frosting conditions by assuming a uniform distribution of frost to develop over the entire external surface. They used the ideal gas theory to calculate the mass of water diffused in the frost layer on a single circuit through which was circulated a 50% ethylene-glycol/water mixture as the refrigerating fluid. (Seker et al., 2004a, 2004b) carried out numerical and experimental investigations on frost formation. The authors used a custom-made heat exchanger on the geometry of which little information is available. The experiments were performed with a large temperature difference (17°C) between air and refrigerant. The authors used a correlation for airside heat transfer, based on their own heat exchanger data which cannot be extrapolated to other coil conditions. (Yang et al., 2006a, 2006b) optimized fin spacing of a frost fin-and-tube evaporator to increase coil performance and operational time between defrost cycles.

In common to most of the theoretical and modeling work reported herein, validations generally relied on the data available in the open literature or on private collaborative exchanges. A limited number however did have their proper validation set-ups, ((Liang et al., 1999), (Bendaoud et al., 2011), (Liang et al., 2000), (Liang et al., 2001), (Seker et al., 2004a, 2004b)).

2.2 Experiments

Relatively, experimental work on finned tube heat exchangers has been more prolific because the complexity of air flow patterns across finned tubes is quite problematic for theoretical treatments. (Rich, 1973) and (Rich, 1975) conducted a systematic study on air side heat transfer and pressure drop on several coils with variable fin spacing and tube rows. (Wang et al., 1996) and (Wang et al., 1997) investigated the effect of fin spacing, fin thickness, number of tube rows on heat transfer and pressure drop with commonly used tube diameters in HVAC coils, under dry and humid conditions respectively. (Chuah et al., 1998) investigated dehumidifying performance of plain fin-and-tube coils. They measured the effects of air and water velocities which they compared to predictions based on existing methods. Regarding frost formation on coils, (Stoecker, 1957) and (Stoecker, 1960) was among the pioneers who recommended using wide fin spacing and over sizing the coils operating under these conditions in order to limit the defrosting frequency. (Ogawa et al., 1993) showed that combining front staging and side staging respectively reduced air flow blockage and promoted more heat transfer at the rear, globally reducing pressure losses and improving performance. (Guo et al., 2008) conducted their study on the relation between frost growth and the dynamic performance of a heat pump system. They distinguished three stages in frost build up, which they related to the capacity and COP of the heat pump. They found that performance declined rapidly in the third stage during which a fluffy frost layer was formed, particularly when the outdoor temperature was near 0°C. Last but not least is the work reported by (Aljuwayhel et al., 2008) about frost build up on a real size evaporator in an industrial refrigeration ammonia system operating below -34 °C. In-situ measurements of temperatures, flow rates and humidity were gathered to assess capacity degradation as a result of frost. Capacity losses as high as 26%, were recorded after 42 hours of operation. A detailed review of plate fin-and-tube refrigeration heat exchangers is beyond the scope of this paper, because some new material on circuit and frost modeling, as well as analysis results will be introduced. For a detailed review of operational details and data under different conditions, the reader is referred to (Seker et al., 2004a, 2004b), (Wang et al., 1996) and (Wang et al., 1997).

3. Research at CanmetENERGY

3.1 Theoretical approach

Two essential and most uncertain coil design parameters are the heat transfer coefficients and the pressure losses on both air and refrigerant sides. Their theoretical assessment requires rather involved mathematics due to the coupling of heat, mass and momentum transfer as well as geometry, thermo physical and material aspects. As a result of this complexity, the various geometric configurations, the different fin types and arrangements, the design has been generally empirical, relying on experimental data, graphical information and or correlations. (Kays&London, 1984) expressed this information in terms of the Colburn j and f friction factors, which now form the basis for all the subsequent empirical and semi-empirical work currently available. As a consequence, heat exchanger analysis treats traditionally the design and the rating as two separate problems. However, due to the new developments in modeling and simulation techniques, supported by the modern computational power, it is possible to effectively tackle the two aspects simultaneously, to yield both a satisfactory design and knowledge of its sensitivity to geometric and specification changes. Working along the lines of lifting to as large extent as possible the limitations imposed by empirical techniques, an extensive research and development program was set at the laboratories of Natural Resources Canada with the objectives of developing detailed models for coil design and simulation in the context of dry or frosting conditions. Complementary to the theoretical work, a fully instrumented test bench was built to generate data in a large interval of operating conditions. However, a comprehensive experimental study of coil performance under various conditions remains expensive because of the high costs related the large number of possible test configurations and operator time. Numerical modeling, on the other hand has the potential of offering flexible and cost-effective means for the investigation. A typical refrigeration coil sample is represented in (Fig. 1). Refrigeration coils are generally arranged in the form of several circuits. This study focused on CO_2 coils employed in low temperature secondary loops. Air flows on the outside, across the finned coil and carbon dioxide flows inside the tube. Aluminum fins of wavy, rectangular shape are assembled on the copper tubes.

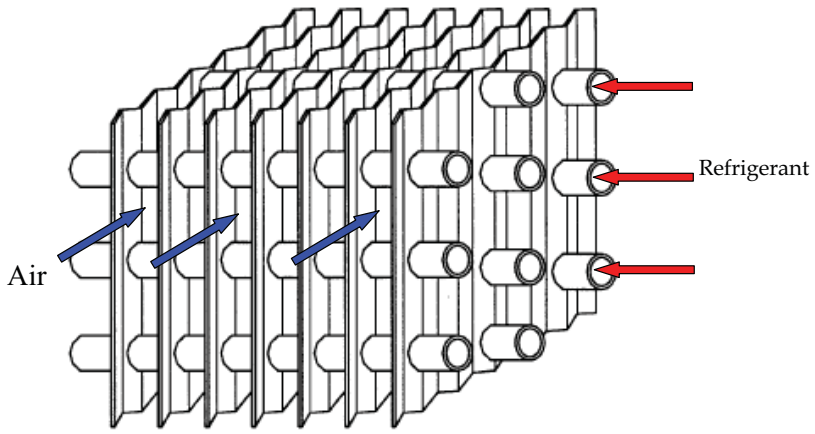

Fig. 1. Schematic of a typical refrigeration evaporator coil

Model development to design coils with different geometric configurations and simulate their thermal hydraulic behaviour revolved around similar geometries. They were performed in two steps: the first development by (Ouzzane &Aidoun, 2008) handled dry cases and the second one by (Bendaoud et al., 2011) was for coils with frost formation. The approach consisted in dividing the heat exchanger into incremental elements over which fundamental conservation equations of mass, momentum and energy were applied (Fig.2).

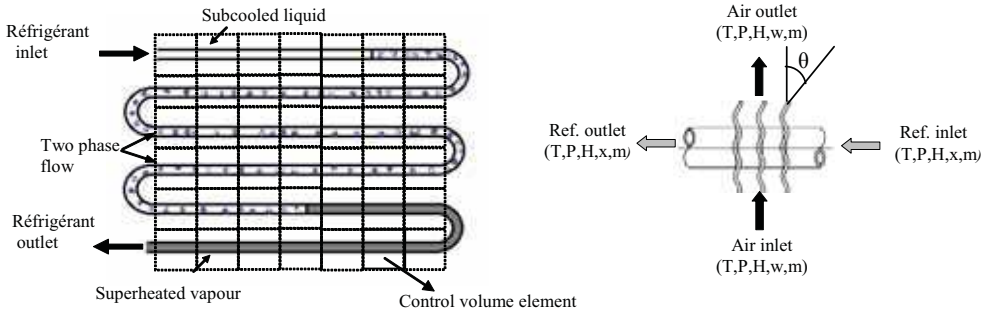

a) Evaporation process and mesh grid b) Control volume element

Fig. 2. Evaporator coil and discretization

3.1.1 Main assumptions

- One dimensional flow of refrigerant inside the tube coil.
- Gravity forces for both air and refrigerant neglected.
- Negligible heat losses to the surroundings.
- Uniform air velocity across each tube row.
- System in steady and quasi-steady state conditions for dry and frosting conditions respectively.
- Uniform frost distribution on the entire control volume and the frost layer, characterised by average properties.

3.1.2 Conservation equations and correlations

Conservation equations of mass, momentum and energy are successively applied to a control volume element (Fig. 2). The resulting relations are summarized as:

Equation of mass

$$\left(\sum \dot{m}_r\right)_{ou} = \left(\sum \dot{m}_r\right)_{in} \text{ and } \left(\dot{m}_a\right)_{ou} = \left(\dot{m}_a\right)_{in} \tag{1}$$

Equation of momentum

Pressure losses are calculated in tubes and return bends as follows:
For tubes:

$$\left(P_r\right)_{ou} = \left(P_r\right)_{in} - \left(\Delta P_r\right)_l \tag{2a}$$

For return bends:

$$\left(P_r\right)_{ou} = \left(P_r\right)_{in} - \left(\Delta P_r\right)_b \tag{2b}$$

For single phase, subcooled liquid and superheated vapour, the Darcy-Weisbach equation is used to calculate the linear pressure drop as:

$$\left(\Delta P_r\right)_l = f.\Delta L.\frac{8.(\dot{m}_r)^2}{\rho_r.\pi^2.D_{in}^5} \tag{3}$$

The friction factor f is calculated by using the correlation given by (Drew et al., 1932)
Pressure losses in bends are calculated by:

$$\left(\Delta P_r\right)_b = f_b.\frac{8.(\dot{m}_r)^2}{\rho_r.\pi^2.D_{in}^4} \tag{4}$$

Where, the friction coefficient f_b is given by (Kays &London, 1984).
For two phase flow the linear pressure drop is calculated by the equation:

$$\left(\Delta P_r\right)_l = \left[\frac{f}{2.D_{in}}\Delta L.\nu_{tp(ou)} + \left(\nu_{tp(ou)} - \nu_{tp(in)}\right)\right]G^2 \tag{5}$$

With G being the mass flow rate per unit area, and f being the friction factor coefficient determined on the basis of the homogeneous model reported by (Rohsenow et al., 1998). Two-phase pressure drop in bends is based on the correlations due to (Geary, 1975).

$$\left(\Delta P_r\right)_b = \left(f_b\right)_{tp}.\frac{L_b.x^2.G^2}{2.\left(\rho_r\right)_g.D_{in}} \tag{6}$$

L_b is the length of the bend, and $(f_b)_{tp}$ is the friction factor for a return bend calculated by:

$$\left(f_b\right)_{tp} = \frac{80352.10^{-8}.Re_g^{0.5}}{\exp(0.215.C_d / D_{in}).x^{1.25}} \tag{7}$$

Where C_d is the bend's centre-to-centre distance and Re_g is the Reynolds number based on the refrigerant vapour phase.

Equation of energy

The equations resulting from the energy balance are summarized as:

$$\dot{Q} = \dot{m}_r.\left[\left(H_r\right)_{ou} - \left(H_r\right)_{in}\right] \tag{8a}$$

$$\dot{Q} = \dot{m}_a.\left[\left(H_a\right)_{in} - \left(H_a\right)_{ou}\right] \tag{8b}$$

and

$$\dot{Q} = h_r.A_{in}(\overline{T_w} - \overline{T_r}) \tag{9a}$$

$$\dot{Q} = h_a.A_{ou}\left(\overline{T_a} - \overline{T_w}\right) \tag{9b}$$

$\dot{Q}$ is the heat transfer rate, h_r and h_a the heat transfer coefficients for the refrigerant and air, respectively.

Heat transfer coefficient for CO_2

For single phase, the heat transfer coefficient h_r is calculated using the correlation proposed by Petukhov and Kirillov reported by (Kakaç et al., 1998). For two phase flow, the correlations developed by Bennet-Chen and modified by (Hwang et al., 1997) were used to calculate h_r. This is based on the superposition principle, which consists of assuming that h_r is the sum of nucleate boiling coefficient h_{nb} and convection heat transfer coefficient h_{bc} as:

$$h_r = h_{nb} + h_{bc} \tag{10}$$

Where h_{nb} and h_{bc} are given respectively by:

$$h_{nb} = \Omega.\left(T_w - T_{sat}\left(P_l\right)\right)^{0.4}.\left(P_{sat}\left(T_w\right) - P_l\right)^{0.75}.S \tag{11}$$

And

$$h_{bc} = h_l.Pr^{0.6}.F.(1-x)^{0.8} \tag{12}$$

h_l is the convective heat transfer coefficient for the liquid phase, calculated by Dittus-Boelter correlation (Incropera et al., 2002). The expressions of Ω, S and Fin equations (11) and (12) can be found in (Hwang et al., 1997).

Air side heat transfer coefficient

For air flowing over wavy plate-finned tubes, the (Wang et al., 2002) correlations for heat transfer and pressure drop are used. Heat transfer is expressed by the Colburn coefficient as:

$$J = 0.0646.Re_{Dc}^{J_1}.\left(\frac{D_c}{D_h}\right)^{J_2}.\left(\frac{F_s}{S_t}\right)^{-1.03}\left(\frac{S_1}{D_c}\right)^{0.432}.J_3 \tag{13a}$$

And

$$J = \frac{h_a.D_c}{k_a.Re_{Dc}.Pr_a^{1/3}} \tag{13b}$$

D_c and D_h are the fin collar outside and the hydraulic diameters respectively.
The pressure drop across the coil can be computed by the expression proposed by (Kays &London, 1984)

$$\Delta P_a = \frac{G_{max}^2}{2\rho_{a,in}}\left[f_a\left(\frac{A_c}{A_{min}}.\frac{\rho_{a,in}}{\rho_m}\right) + \left(\left(1+\beta^2\right)\left(\frac{\rho_{a,in}}{\rho_{a,ou}} - 1\right)\right)\right] \tag{14}$$

ρ_m is calculated at the mean temperature between air inlet and outlet.
A_c : total air side heat transfer area.

A_{min}: minimum free flow area through which air passes across the coil.
β: ratio of free-flow to frontal area.
The air friction factor f_a is calculated by the correlation proposed by (Wang et al., 2002)

$$f_a = 0.228\,Re_{Dc}^{fl}.(\tan\theta)^{f2}\left(\frac{F_s}{S_1}\right)^{f3}\left(\frac{S_1}{D_c}\right)^{f4}.f_5 \tag{14a}$$

Air properties are calculated using the standard psychometric relations (ASHRAE, 1993).
Expressions for J_1, J_2, f_1, f_2, f_3, f_4 and f_5 are given in (Wang et al., 2002).
The rate of frost formation is expressed as a loss of humidity as water vapour condenses on the cold coil surface.

$$m_f = m_{da}.(\omega_{in} - \omega_{ou}).\Delta t \tag{15}$$

The mass of the dry air is expressed as:

$$m_{da} = \frac{\dot{m}_t.\Delta t}{1+\omega_{in}} \tag{16}$$

Frost properties

The frost distribution on the entire control volume is assumed to be uniform, and the frost layer is characterised by average properties. When the saturated air passes over the coil surface at a temperature below the dew point, the first frost layer appears. The initial conditions for frost height and density are important as the results are sensitive to their selection (Shokouhmand et al., 2009). (Jones & Parker, 1975) tested the initial conditions by changing the values of the initial frost thickness and density, they found that the prediction results of the frost growth rate would not be affected significantly if the initial frost thickness approaches a low value (~ 2 x 10^{-2} mm). They also found that as long as the initial value of the frost density is significantly smaller than the frost density during growth, it will not affect the solution for the frost growth rate of densification, the recommended value being (~ 30 kg.m^{-3}). Hence, in this work, the initial conditions for the frost temperature, thickness and density are fixed as:

$$T_f^0 = T_w \quad , \quad \delta_f^0 = 2.10^{-5}\,m \quad , \quad \rho_f^0 = 30\ kg/m^3$$

The water vapour transferred, from moist air to the frost surface, increases both the frost density and thickness. This phenomenon can be expressed as:

$$m_f = m_\delta + m_\rho \tag{17}$$

The mass flux from the frost density absorbed into the frost layer is given by (Lee et al., 1997):

$$m_\rho = \int_{\delta_f=0}^{\delta_f=Y_f} \alpha_f \rho_w.\Delta t.d\delta_f \tag{18}$$

Were α_f represents an absorption coefficient calculated by:

$$\alpha_f = D_v.\left[\frac{\cosh^{-1}}{\delta_f}\left\{\frac{\rho_{w,sat}\left(T_{f,s}\right)}{\rho_{w,sat}\left(T_w\right)}\right\}\right]^2 \tag{19}$$

The thermal conductivity, valid for $30 \le \rho_f \le 400 \quad kg.m^{-3}$, is given by:

$$k_f = 0.132 + 3.13.10^{-4}.\rho_f + 1.6.10^{-7}.\rho_f^2 \tag{20}$$

The diffusion coefficient D_v is valid for $-50 \le \overline{T}_a \le +20\,^{\circ}C$ and is given by:

$$D_v = \left(a + b\overline{T}_a + c\overline{T}_a^2 + d\overline{T}_a^3\right).10^{-5} \tag{21}$$

With:

a = 2.219928, b = 0.0137779, c = -0.0000065, d = $-5.32937434.10^{-7}$

The frost density and thickness for each time interval are calculated as follows, (Kondepudi et al., 1993a):

$$\Delta\rho_f = \frac{\dot{m}_\rho\,\Delta t}{A_{c,d}\delta_f} \tag{22}$$

$$\Delta\delta_f = \frac{\dot{m}_\delta\,\Delta t}{A_{c,d}\rho_f} \tag{23}$$

$A_{c,d}$: convective heat transfer area in dry condition.

3.1.3 Solution procedure

Two different solution procedures were developed in the modeling process: Forward Marching Technique (FMT) (Ouzzane & Aidoun, 2004) and Iterative Solution for Whole System (ISWS) (Bendaoud et al., 2010). The Forward Marching Technique allowed local tracking of relevant operational parameters. Differential lengths of tubing were used where single phase flow prevailed and differential variations of quality were employed in zones of two-phase flow. Taking advantage of the relative flexibility offered by this technique, it was upgraded by (Aidoun & Ouzzane, 2009) to handle simple circuitry. In this case the method calls for iterations where a guess on the refrigerant conditions at exit is made and the inlet conditions are calculated. These are compared to the fixed inlet conditions. Iterations are repeated until convergence between fixed and computed inlet conditions are met. The ISWS procedure is intended to cover a large range of operating conditions and handle complex circuiting configurations. In order to achieve this objective, the solution procedure is based on the adoption of an original strategy for the convention of numbering and localizing the tubes, identifying refrigerant entries, exits, tube connections, as well as control volume variables. Rows are counted according to the air flow direction.

J(I,K) is a matrix indicating the presence or absence of a junction between two tubes; the coordinates I and K indicate the direction of flow: incoming and destination, respectively. The values of J(I,K) are:

$$J(I,K)=\begin{cases}0 & \text{no connection between I and K tubes}\\ 1 & \text{connection between I and K tubes}\end{cases}$$

Index 1 for I or K is allowed only for the exit or entry to the system. (Fig. 3) shows an example of a heat exchanger with 9 tubes arranged in three rows and three lines with one entrance in tube 5 and two exits in tubes 2 and 10. J(1,5) means that the refrigerant enters in tube 5. J(2,1) and J(10,1)) indicate exits from tubes 2 and 10 respectively. J(4,3) is the junction between tubes 4 and 3 and the flow is from tube 4 through to tube 3.

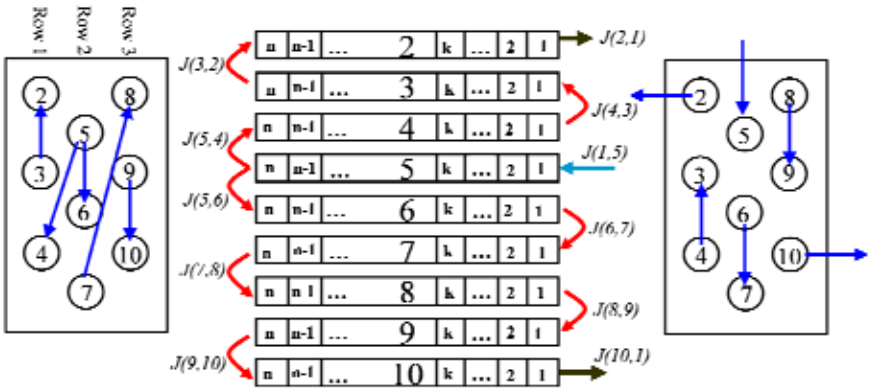

Fig. 3. An example of circuiting configuration with volume control elements and conventions

Each tube I is divided into n control volume elements, starting either from the left or from the right, depending on the refrigerant flow direction entrance. For this purpose, a parameter DIR(I) having a value of 1 or -1 is allocated to each tube. In (Fig. 3), the direction of the upper entrance tube is chosen as a positive reference (DIR(I)=1). In this way, DIR(5)=DIR(3)=DIR(7)=DIR(9)= +1 and DIR(2)=DIR(4)=DIR(6)=DIR(8)=DIR(10)= -1. As for FMT, the resolution still relies on an iterative method but it is applied on matrix system.The main steps of theses two computing procedures are indicated in the flow charts of (Fig. 4) and (Fig.5). Geometric and operation data are first introduced, then the thermodynamic state of the refrigerant is defined (at the outlet for FMT and at the inlet for ISWS), using subroutine REFPROP (NIST, 1998). Three cases are possible:

- Two-phase: calculations are made according to the steps on the right branch of the flowchart.
- Superheat for FMT or subcooling for ISWS: the case is treated according to the steps on the left branch.
- Subcooling for FMT or superheat for: no calculations are performed since there is no evaporation.

If operating under frost condition with ISWS (Fig. 5) and when hydrodynamic and thermal convergence is obtained, the subroutine HUMI is called to compute the air relative humidity at inlet and outlet of each volume element. Data are stored in matrices $[\Phi_{in}]$ and $[\Phi_{ou}]$ respectively. The program then checks, for each volume element if the conditions of frost formation are verified, i.e. saturated air and T_s below the freezing point. For the elements under the dew point temperature, the subroutine computes the mass of the frost formed,

distributed into diffused (m_ρ) and solidified (m_δ) mass parts. Next, the program calls the subroutine UPCOILGEO to update the geometric configuration of the heat exchanger (outer tube diameter, fin thickness, convective heat transfer area, free flow area) and stores the information in respective matrices. By considering the most recent geometry resulting from frost deposition over a time step, the hydrodynamic, thermal and psychometric calculations are repeated for each time step Δt until the total working period of the heat exchanger is covered.

3.2 Experimental validation

In the first instance, results from the FMT and ISWS procedures were compared as part of the model validation process. For dry and frosting conditions further comparison was respectively performed with the available information from the literature (Kondepudi et al., 1993b) and with data from the CanmetENERGY's experimental stand (Ouzzane & Aidoun, 2008). This installation, shown in (Fig.6), complies with ASHRAE standards for forced air cooling and heating coils (ASHRAE, 2000). Evaporating carbon dioxide is the working fluid in the loop of interest (L1), which includes a CO_2 pump, a mass flow meter, a CO_2-air coil with aluminum wavy fins and copper tubes, a brazed plate condenser and a reservoir for CO_2 condensate. The loop is well instrumented for the purpose of heat and mass transfer balances and fluid flow. For a flexible control of temperature and capacity, a brine loop (L2) was used to cool down the CO_2 condenser. The temperature control of this loop is achieved by a mechanical refrigeration system (L3). Loop (L1) is located in a closed room with two compartments corresponding to inlet and outlet of the coil: air flows from one compartment to the other through a duct enclosing the coil. Air circulation is maintained by a blower. The compartments are well insulated in order to reduce infiltration of outside air and moisture.

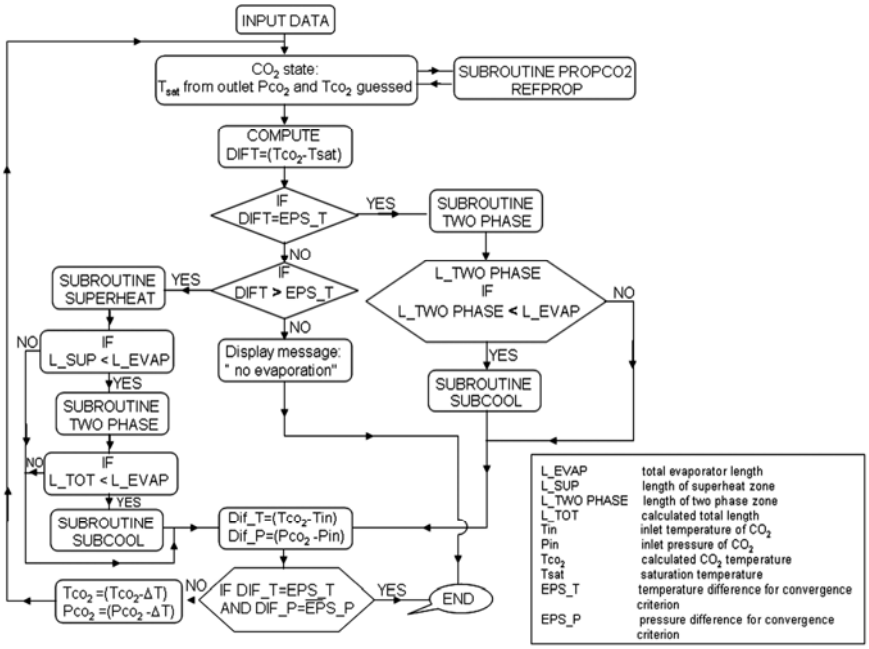

Fig. 4. Flow chart of the computing procedure for FMT

Means of adjusting air temperature and humidity conditions at the duct inlet are provided by a brine cooler, electric heating and a steam generator. Both compartments are equipped with temperature, pressure, flow and dew point sensors set in accordance with ASHRAE standards (ASHRAE, 1987). The coil is 0.22 m deep with a face area of 0.61m x 0.32 m. The configuration employed is similar to that represented on Figure1 and has eight rows of ten tubes, 8.7 mm internal diameter, 4 fins per inch, arranged in one circuit.

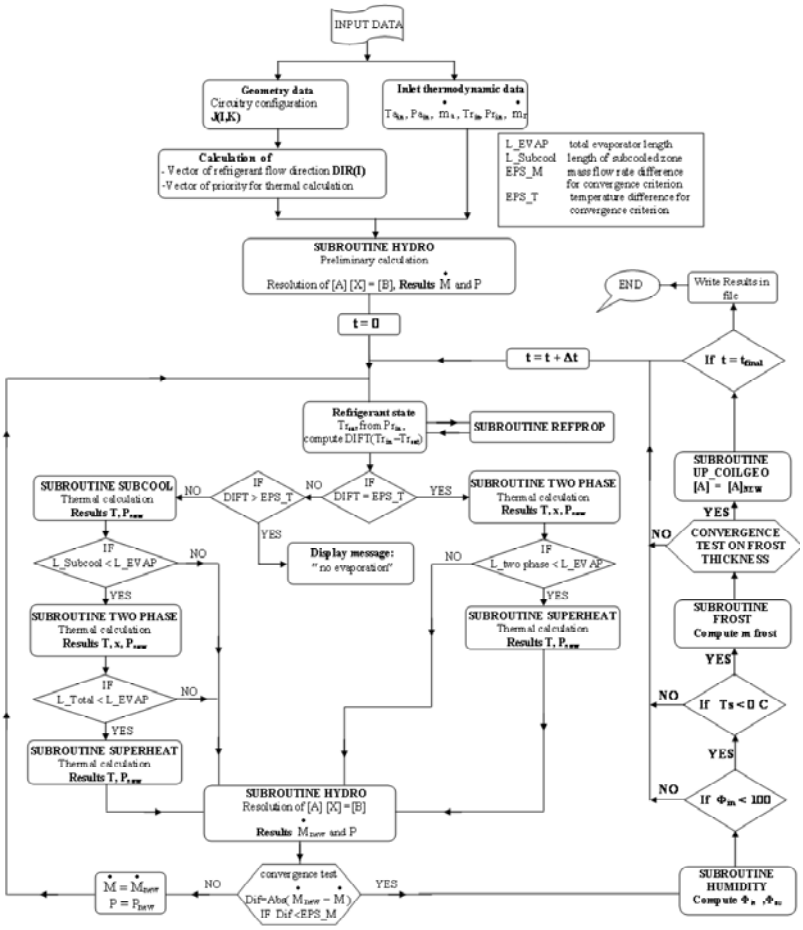

Fig. 5. Flow chart of the computing procedure for ISWS

At temperatures of -10 ºC and -15 ºC as used here, air absorbs only a very low quantity of vapour. Therefore, it is very difficult to vary and to control air humidity at the evaporator coil entrance. The steam injected in the test chamber instantaneously freezes on the walls and injector orifice. For this reason the injection system is designed to ensure sufficient steam superheat and residence time for it to be absorbed by the ambient air. (Fig. 7) shows a schematic of the steam injection. Saturated vapour produced in the generator flows in an insulated pipe to an electrical superheater. The desired level of superheat and the required

steam quantities result from a combined adjustment of the heaters and the solenoid valves for the steam injection and water drainage. Operation of the heaters is controlled to ensure the required temperature for the injected steam. Presented below are some comparison examples and validations performed. For dry surfaces, four different experimental cases are selected, with their operating conditions summarized in Table 1.

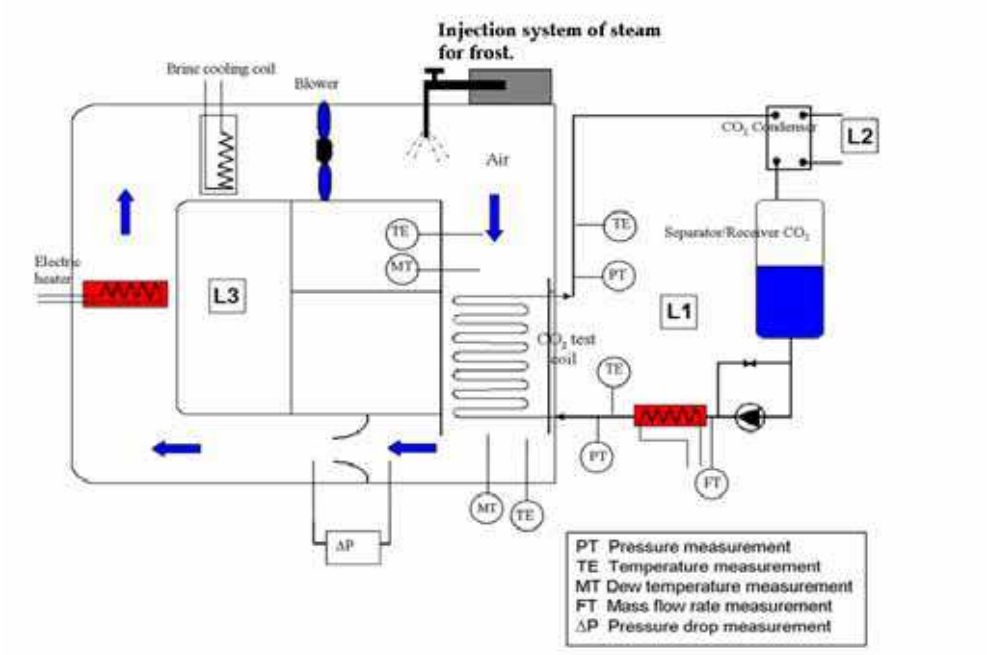

Fig. 6. Schematic diagram of CanmetENERGY test set-up

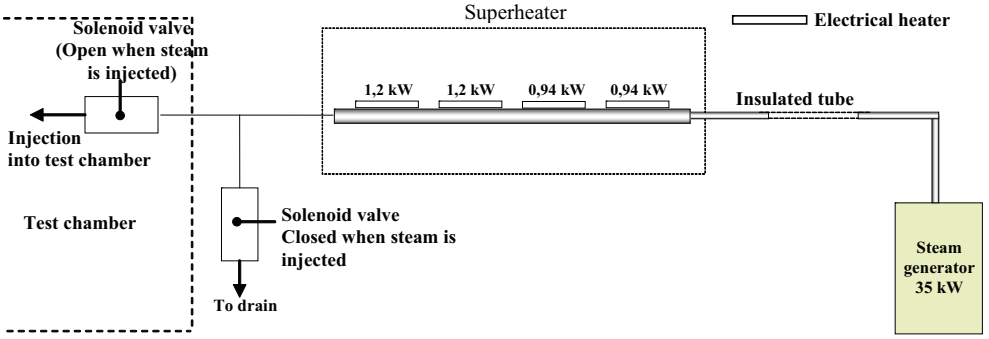

Fig. 7. Schematic of injection system of steam

In all these cases, the refrigerant is entering the coil in a saturated state with an assumed quality of 0 %. The results in Table 2 show that the coil capacity predicted by the ISWS procedure is in good agreement with the experimental data, the maximum discrepancy

being less than 6.5 %. Comparison with FMT procedure of (Ouzzane & Aidoun, 2008) shows differences of less than 14 %.

	Mass flow rate (kG/s)		Inlet temperature (°C)		Inlet pressure (kPa)	
	Air	CO_2	Air	CO_2	Air	CO_2
CASE 1	0.5865	0.02700	-15.5	-26.07	101.325	1624.7
CASE 2	0.6070	0.01864	-15.6	-26.93	101.325	1580.5
CASE 3	0.5865	0.01619	-16.0	-27.29	101.325	1560.3
CASE 4	0.6090	0.01472	-20.3	-24.03	101.325	1732.8

Table 1. Input conditions for validation

The results show also that the refrigerant pressure drop predicted by ISWS procedure is in good agreement with the experimental data. The cumulative errors resulting from the iterative process applied with correlations for pressure drop whose overall uncertainty is ± 50% (Rohsenow et al., 1998) and for the heat transfer coefficient whose uncertainty on the predictions is ± 40 % (Hwang et al., 1997) are well within the acceptable range. In the analysis performed by (Ouzzane & Aidoun, 2008), the pressure drop for the saturated refrigerant flow is strongly affected by the quality of the refrigerant. Since the iterative process in the present approach is based on tube length increments, and because quality results from computations, it is possible that surges in quality occur towards the end of the evaporation process and result in correspondingly high departures of the pressure drop outside the range covered by the correlations used.

		Capacity (W)		Outlet quality	ΔP (kPa)	Outlet temperature (°C)		Outlet relative humidity (%)
		Air	CO_2	CO_2	CO_2	Air	CO_2	Air
CASE 1	ISWS	4091.0	4112.9	52.8 %	170.2	-22.4	-29.4	-
	FMT	4438.3	4530.6	58.0 %	195.2	-23.0	-29.9	-
	Experiments	4083.3	-	51.4 %	171.6	-22.4	-29.6	66.0
CASE 2	ISWS	4444.6	4435.2	80.7 %	152.5	-22.9	-30.0	-
	FMT	4811.5	4914.1	89.0 %	149.6	-23.5	-29.9	-
	Experiments	4471.0	-	75.0 %	132.2	-22.9	-29.6	65.6
CASE 3	ISWS	1402.4	1379.1	32.5 %	29.3	-22.6	-24.5	-
	FMT	1557.2	1550.0	36.5 %	38.6	-22.8	-24.8	-
	Experiments	1495.9	-	35.5 %	44.4	-22.7	-24.9	76.0
CASE 4	ISWS	5588.8	5590.6	45.3%	195.0	-19.4	-26.6	-
	FMT	5869.4	5683.8	47.5%	398.9	-19.8	-30.8	-
	Experiments	5458.0	-	43.5 %	303.4	-19.1	-28.8	54.7

Table 2. Comparison of numerical results from two resolution procedures and experiments

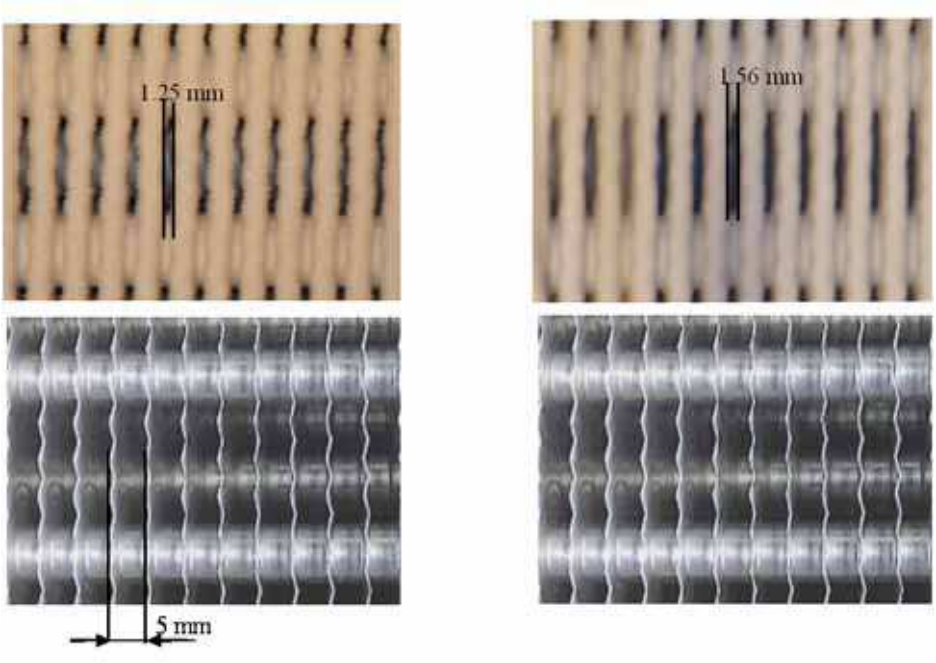

Fig. 8. Pictures showing the frost formed on tubes and fins

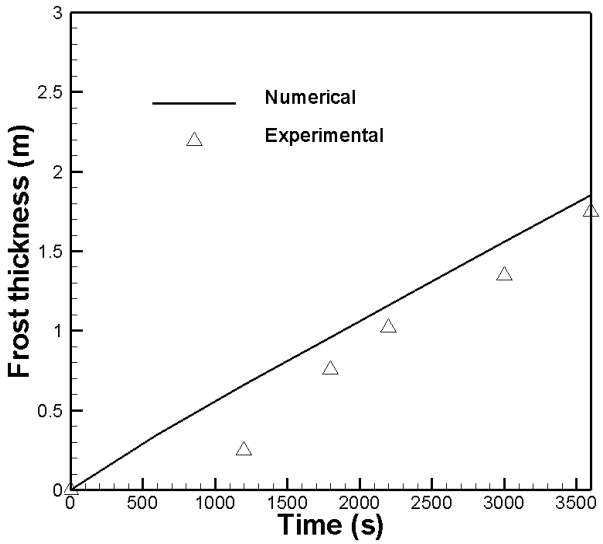

Fig. 9. Variation of the frost thickness with time

Under frosting conditions, several tests were performed on the test bench at CanmetENERGY, some of which were selected to validate the theoretical model. From the pictures taken by digital cameras located at the inlet and outlet of the coil (Fig. 8), the frost thickness is estimated. The coil with no frost is used as a reference for the scale and the frost thickness variation with time is shown in (Fig. 8).

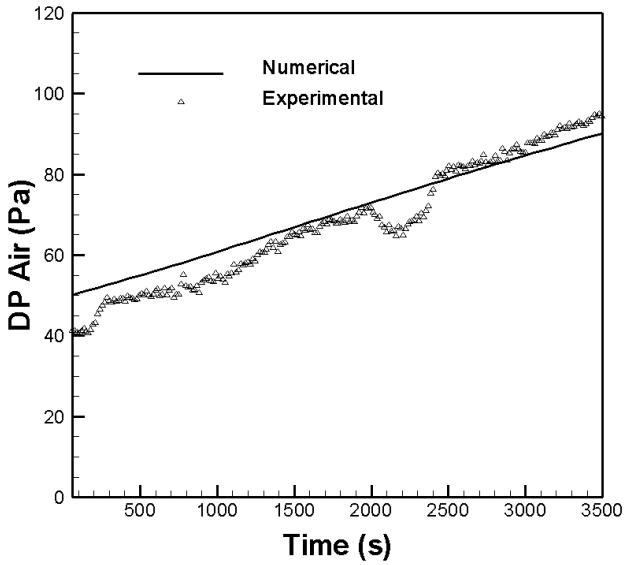

Fig. 10. Variation of the air pressure drop with time

Variations of the frost thickness and air pressure drop with time are presented in Fig. 9 and Fig. 10. As frost accumulates air flow passage cross-sections reduce, thereby increasing the pressure drop. Agreement between experimental and numerical calculations is quite satisfactory. The first measurable frost layer thickness is only observed after 20 minutes from the start. This is due to difficulties in accurately estimating slowly developing frost layer thicknesses.

4. Simulation results

The developed theoretical tool using FMT and ISWS procedures was used to perform several studies. An interesting feature is that all relevant operation parameters can be determined locally along the coil and mapped. In the example represented in (Fig. 11), typical results are shown for the air temperature from inlet to outlet, row after row. The general tendency towards temperature decrease with the row number can be expected but the distribution along tube lines is less obvious and will depend on the configuration and the operating conditions. In the first and the last rows (A-A and D-D sections), we can clearly see zones where single phase refrigerant prevails. Subcooled liquid and superheated vapour, are represented in blue and red respectively. The same kind of results can be presented for relative humidity (Ouzzane & Aidoun, 2004), in which case the locations where frost formation may first develop are indicated.

4.1 Effect of recirculation

Experience from large ammonia refrigeration installations reveals that circulation makes better use of the evaporators' surfaces, with enhanced heat transfer and improved overall system performance. This technique is now being proposed in more modest sizes as well, by inserting an accumulator in the system. In these systems a separator supplies liquid refrigerant to the evaporator while saturated vapour is fed to the compressor. At the evaporator exit saturated refrigerant in the state of liquid-vapour mixture is sent back to the separator (x<1). The overall impact is a performance improvement through a refrigerant flow rate increase (with a corresponding internal heat exchange improvement) and a reduction or elimination of superheat at the compressor suction.

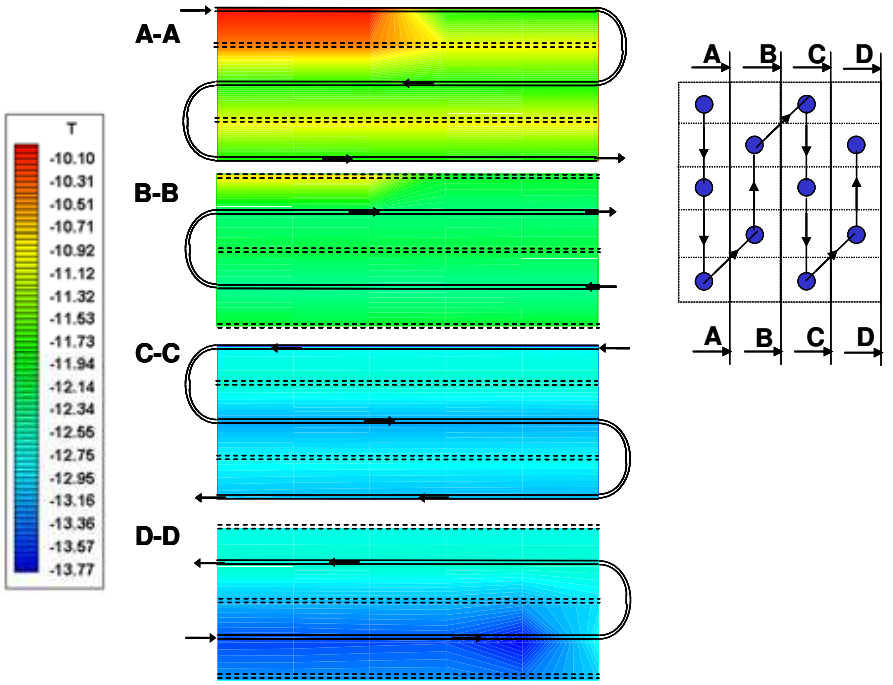

Fig. 11. Typical temperature field inside the coil

However this improvement comes with saturation pressure and related temperature variations, resulting in property values reductions. These opposing effects are expected to lead to an optimum circulation ratio with traditional refrigerants and ammonia. Using an actual installation to obtain data however, imposes limitations on their range and on the extent of the corresponding parametric analysis that will be derived. In (Ouzzane & Aidoun, 2007), circulation of CO_2 was studied as part of secondary loops with phase change, as found in supermarkets. The purpose was to investigate the impact of the circulation practice on heat transfer and heat exchangers performance, through modeling and test bench data for CO_2. In the first instance this will be limited to the evaporator. The circulation ratio, N was varied in the range 1 to 4 and corresponding heat transfer coefficients, internal pressure drop and saturation temperature variations were obtained. Despite a substantial

improvement in heat transfer due to circulation (in the order of 180% for N=4), the coil capacity remained almost unchanged while pressure drop considerably increased and the corresponding saturation temperature dropped from 1.7 °C for N=1 to 6.4 °C for N=4. In the following analysis and discussion, two sets of results will be considered. The first set comes from experiments performed on a test bench with coil characteristics specified in the previous section. The second set of results comes from simulations. Since the purpose of this investigation is to study the evaporator coil under the conditions of circulation, operating conditions are adjusted so that only two-phase flow exists ($0 < x < 1$). The range of circulation ratios covered experimentally was from 1 to 5.5 approximately. The coil geometric specifications are those reported in the above section and operating conditions as well as resulting performance parameters are recapitulated in Table 3. On the airside temperature and flow rate were maintained approximately constant. On the CO_2 side saturation conditions (pressure and temperature) were also maintained approximately constant while the flow rate was progressively increased. Assuming negligible heat losses to the surrounding, a heat balance on air and CO_2 allows estimating coil capacity and exit quality, while pressure drop results from direct measurement. The coil capacity appears to be quasi-constant despite some fluctuations around 1.5 kW at these conditions. Bearing in mind that the amplitude of these fluctuations is within the uncertainty range of the measurements and because of the limited number of data points it is not possible at this stage to identify a variation tendency.

	Circulation ratio	N=1.0	N=1.23	N=1.50	N=2.90	N=5.42
CO_2	Mass flow rate (g/s)	5.1	6.23	7.6	14.7	27.5
	Tin (C)	-24.1	-24.3	-24.1	-24.1	-24.1
	x (%) (exit)	100.0	82.8	68.8	36.2	19.7
	ΔP (kPa)	10.0	19.5	27.8	45.3	78.1
Air	$Tair_{in}$ (C)	-20.0	-19.95	-20.0	-20.2	-20.3
	Mass flow rate (g/s)	605.1	589	605.7	606.4	603.1
	Capacity (kW)	1.48	1.501	1.521	1.534	1.514

Table 3. Results from measurement for different circulation ratios

The pressure drop on the other hand increases very rapidly with circulation ratio. Further investigation of this effect was performed by simulation of a typical refrigeration case for supermarket conditions. The coil operating conditions and the corresponding results are summarized in Table 4 for circulation ratios ranging from 1 to 4.

Circulation affects positively the refrigerant side heat transfer coefficient, as is shown by (Fig. 12). This is due to the combination of good thermo physical properties of CO_2 and

increasing flow rates. The increase is at least 85% when going from N=1 to N=4. However, the maximum local increase of the overall heat transfer coefficient is no more than 10% (Ouzzane & Aidoun, 2007).

Geometry and conditions		Circulation ratio	1	2	3	4
Inner diameter = 8.7mm Ext. diameter = 9.5mm Fins (27.8×31.8×0.19) 118 fins/m, L = 90 m T_{co2}=-30C, $Tair_{in}$=-24C $\dot{m}_{air} = 1.105\,(kG/s)$	CO_2	$\dot{m}_{CO2}(g/s)$	11.6	23.2	34.8	46.4
		x (%) (exit)	99.66	55.48	37.99	29.89
		ΔP (kPa)	82.66	164.02	220.74	288.26
		Q (kW)	3.551	3.774	3.749	3.672
		ΔT_{CO2}	1.744	3.533	4.81	6.3944

Table 4. Calculation results for different circulation ratios

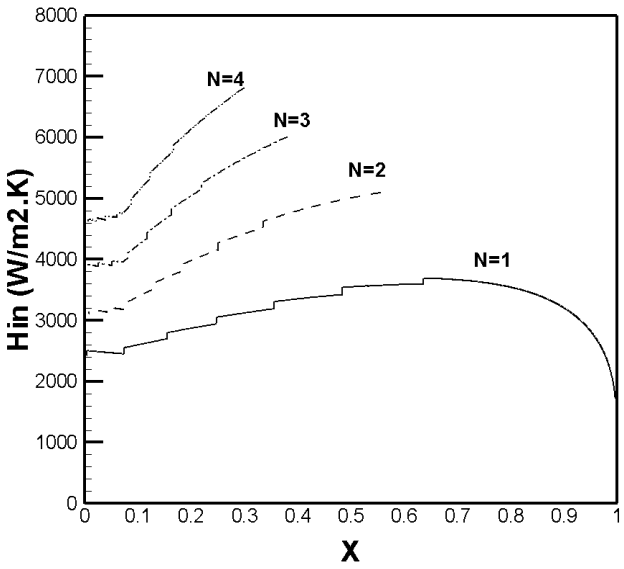

Fig. 12. Internal heat transfer coefficient distribution for different circulation ratios

This is not surprising since the controlling factor is the air side heat transfer, which is known to be limiting. As pointed out earlier, pressure drop increases very rapidly with coil length, (Fig. 13). Up to 90% of this pressure drop occurs in the first half of the coil, particularly for lower circulation ratios, where refrigerant qualities are lower. This study was limited to the coil; however it should be extended to all the system to assess the overall impact.

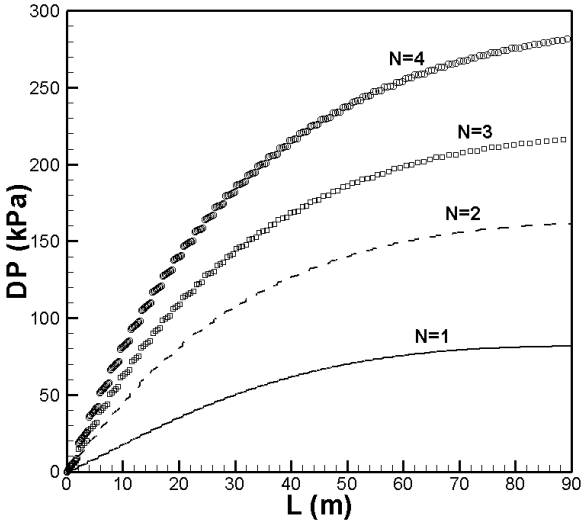

Fig. 13. Internal cumulative pressure drop distribution for different circulation ratios

4.2 Effect of circuiting

Circuiting is an important design factor for performance enhancement, improved flow and air temperature distribution. By combining tube diameter, fin and circuitry arrangements, it is possible to maximise heat transfer per unit volume while minimising flow resistance both internally and externally. Simulations shown in (Fig. 19) and (Fig.20) were obtained for the following conditions: 16 pass coil, T_r=-30 ^{o}C, T_a=-25 ^{o}C and ϕ=50%.

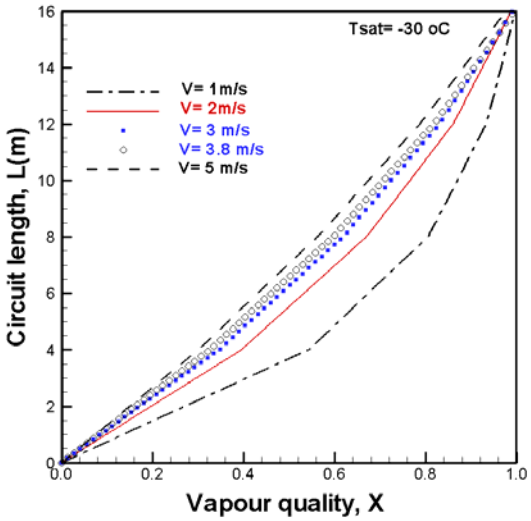

Fig. 14. Distribution of refrigerant quality in the circuit

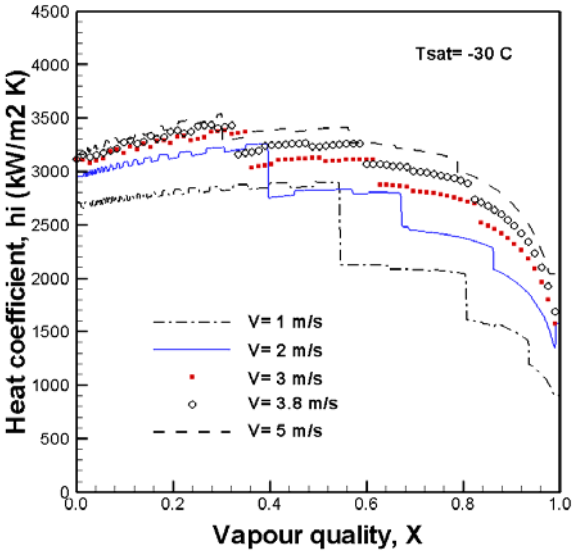

Fig. 15. Heat transfer distribution with quality

(Figure 14) indicates that for $x \geq 0.75$ approximately the required tube length for evaporation increases. For the case considered, 35% of the total length is used in the quality range 0.75 – 1, while only 17.5% is used in the quality range of 0. – 0.25. This is a consequence of more efficient heat transfer in the range of moderate qualities. This condition is expressed in terms of the heat transfer coefficient in figure 15 for different air velocities. The internal heat transfer coefficient h_i on this figure is highest at low qualities and it maintains a stable value up to 50%. From 50% to 75%, its value decreases gradually up to 75%, beyond which the heat transfer declines rapidly, particularly towards 90% quality. On the other hand, it was shown by (Ouzzane & Aidoun, 2005) that internal pressure drop, expressed in terms of the pressure gradient for similar conditions steadily increased in the quality range of $0. \leq x \leq 0.8$ before decreasing again. In the range of qualities $x \leq 0.5$ and $x \geq 0.8$, pressure losses are moderate. Under such conditions it is possible to use high flow rates in the low and high quality ranges for better heat transfer and less pressure loss penalty. The flow may be reduced in the medium range qualities where high heat transfer and high-pressure losses prevail. These important observations are put into practice in the example that follows, where circuiting is expected to play a major role in the design of large capacity coils. Optimized circuits may reduce the coil overall size, better distribute the flow and reduce frost formation. Most hydro fluorocarbons can accommodate only limited tube lengths due to excessive pressure drop in refrigeration coils as is shown for R507A in (Fig. 17), corresponding to the coil geometry of (Fig. 16). Due to the thermo physical properties of R507A, it was found that internal pressure losses were very high, rapidly resulting in a significant drop of saturation temperature over relatively short tube lengths. In order to maintain a reasonably constant temperature across an evaporator this temperature drop must be small (ideally less than 2°C) and in order to fulfill this condition, several short length circuits were needed with synthetic refrigerants, while only one circuit was required with carbon dioxide under similar working conditions (Aidoun & Ouzzane, 2009).

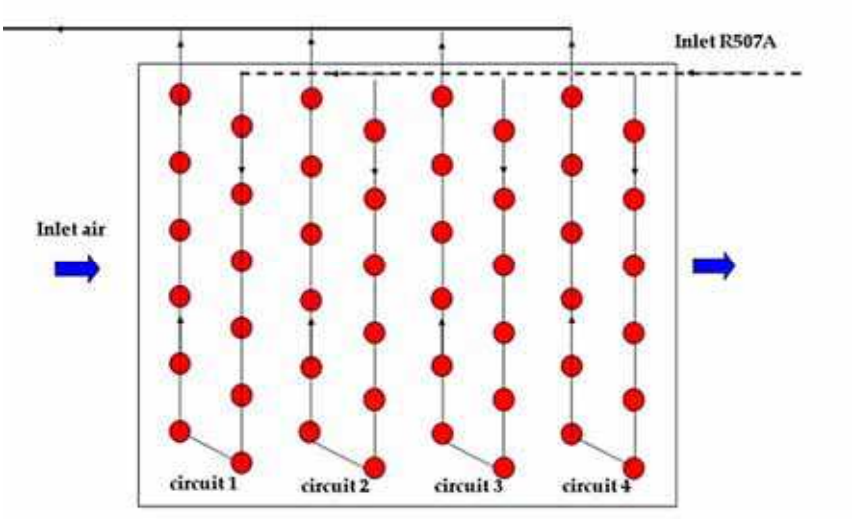

Fig. 16. Case of application for circuiting

In the event of frost formation it is expected to be more uniform and to occur over a longer period of time in comparison to ordinary synthetic refrigerants. With refrigerant R507A, several iterative attempts were performed before obtaining a reasonable temperature drop. At least four circuits were found to be necessary to satisfy this condition. The four circuits selected were 2 rows each, arranged in parallel. In such a case, the circuits are well balanced and the temperature drop in the saturation temperature is of the order of 2.6 ^{o}C in each circuit (22.5 metres) while it's only of the order of 1.8 ^{o}C for CO_2 in all the coil length (90 metres).

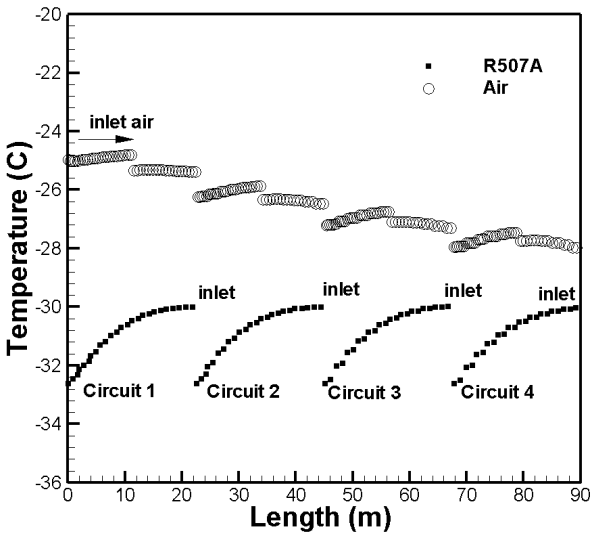

Fig. 17. Temperature distribution for air and R507A with coil length

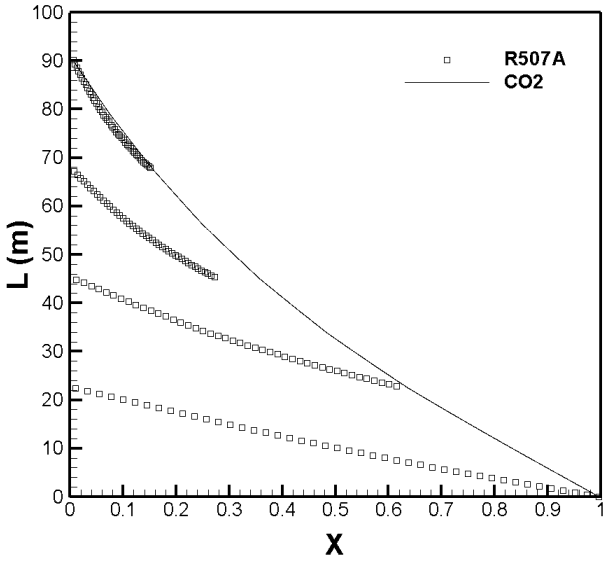

Fig. 18. Evaporation level in different circuits

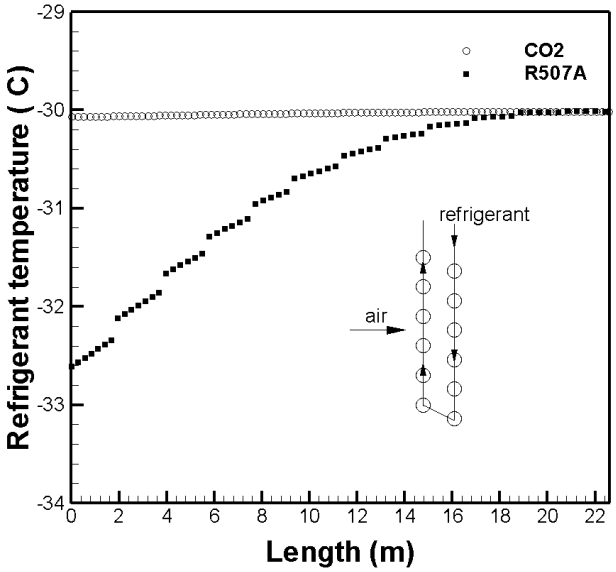

Fig. 19. Effect of refrigerant on temperature glide

(Fig. 18) shows the amount of evaporation taking place in each circuit. CO_2 uses only one circuit and evaporates 100% of the available refrigerant. R505A needs four circuits to deliver the same capacity. In this case only the frontal circuit works at full capacity. The other three are increasingly underused from the coil front to rear because of their exposure to an

increasingly cold air flowing across the coil. In (Fig.19) and considering a representative circuit, the temperature distribution for CO_2 and R507A are compared in the same conditions. Because of its properties, particularly the low viscosity and the high saturation pressure, CO_2 temperature glide with pressure loss is negligible. This in turn insures uniform air cooling and small temperature gradients between refrigerant and air. R507A does not provide the same advantages. The temperature slide is high and as a consequence it is more difficult to obtain uniform air temperature otherwise than by multiplying the number of circuits.

4.3 Effect of refrigerant and geometrical parameters

4.3.1 Effect of refrigerant

Carbon dioxide is considered to be a potential environmentally innocuous replacement in many applications where HCFC'S and HFC'S are currently used. In this context, a comparative study of CO_2, R22 and R134A was performed on a 15 pass, 15 m length staggered counter-current flow tube coil (Aidoun & Ouzzane, 2005). The refrigerant mass flow was adjusted for complete evaporation for R22 which was taken as the reference case. CO_2 was shown to present a very low pressure drop in comparison with R22 and R134a, especially for low saturation temperatures.

Refrigerant	Psat [kPa]	Exit state	Dptotal [Pa]	Q [W]
R22	296.2	x=100 %	4966.2	779.4
CO_2	2288.0	x= 74.5 %	1210.9	726.5
R134A	163.9	x = 91.7%	6486.3	691.6

Table 5. Comparison between different refrigerants

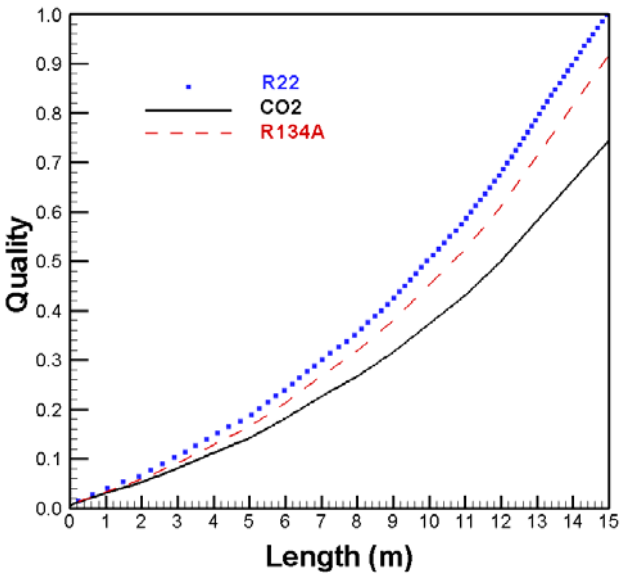

Fig. 20. Quality distribution for different refrigerants

At –20°C, R22 has a pressure drop six times higher than that of CO_2, resulting in higher compression power. (Fig. 20) presents the quality distribution through the tubes for R22, CO_2 and R134A, at -15°C. Air and refrigerant inlet conditions were kept constant. For these conditions, only R22 was completely evaporated (x=1 at exit). The evaporator size is however not sufficient to complete the evaporation of CO_2 and R134A. Due to better internal heat transfer, R22 gives the highest capacity (Table 5). At –15 °C, R134A latent heat of evaporation is comparable to that of R22 (209.5 kJ /kg and 216.5 kJ/kg), respectively. However, because of its other properties, R134A performs less than R22. CO_2 has a comparatively higher latent heat of evaporation (ΔH_L=270.9 kJ/kg]), resulting in the lowest exit quality (x=74.5%). Its lowest pressure drop however allows increasing the mass flow rate with a corresponding increase in heat transfer or decreasing tube diameter.

4.3.2 Effect of fin spacing

Fin spacing was shown to generally enhance heat transfer in dry coils and condensers. Increasing the fin number reduces fin spacing, increases the Reynolds number and the overall heat transfer coefficient. The heat transfer area also increases thereby increasing the heat exchanger capacity and efficiency. When operating at low temperatures the fin number needs to be reduced because of frost formation. Frost build up reduces air flow channels cross section, eventually obstructing them and affects considerably the performance. Overall operation time is reduced because of frequent defrosting, which also means increased energy consumption and decreased production. Simulated results for the conditions of 90% relative humidity and -25 °C evaporation temperature are represented.

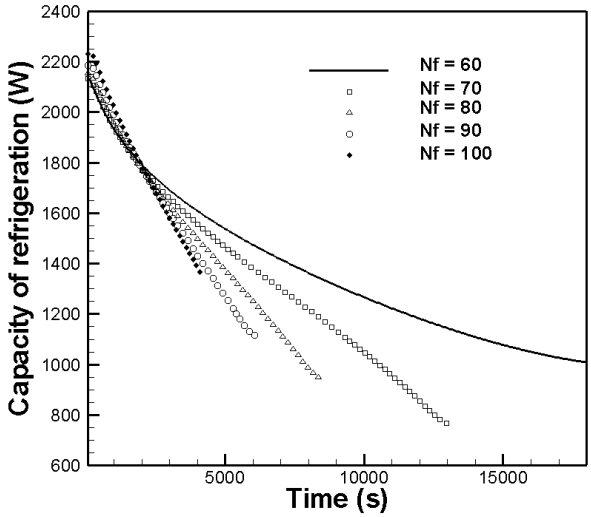

Fig. 21. Cooling capacity for different fin spacing

In this case study, calculations are stopped after five hours of operation or when the first control volume is totally blocked by frost. The effect of fin density on air pressure drop and coil capacity is respectively represented in (Fig. 21) and (Fig. 22). The fin density was varied from 60 to 100, which initially increases capacity but this advantage is lost after approximately 30 minutes due frost growth.

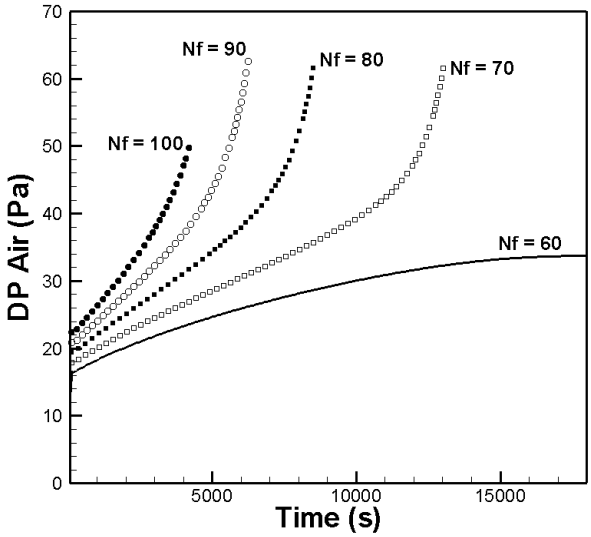

Fig. 22. Air pressure drop for different fin spacing

(Fig. 21) shows heat exchangers with 100 fins per meter get blocked after 66 minutes from the start while those with 60 fins per meter continue to work after 5 hours. (Fig. 21) indicates that as long as the frost layer remains thin, high fin numbers produce more capacity. After approximately 30 minutes of operation, because of the reduction of the exchanger effectiveness which is due to the frost formation, the trend is reversed with the coil having the least fins producing the highest capacity. (Fig. 22) represents air pressure drop in coils with frost development. In this case coils with the highest fin number systematically incur higher losses than those having less fin numbers, irrespective of the amount of frost formed.

4.3.3 Combined effect of tube diameter and circuiting

In order to outline the advantages offered by the combined use of circuiting and CO_2, a comparative study was carried out on two coils with two different tubes diameters: a base configuration (Case A) and circuited configuration (Case B) (Ouzzane & Aidoun, 2008). For Case B and for comparison purposes, the number of tubes and their arrangement are selected in such a way that the frontal section, perpendicular to the air flow is equal to that of Case A. In contrast with Case A (base case) and due to the smaller tube diameter used in Case B, it is not possible to use a single circuit or even two circuits since the pressure losses and the glide of the evaporation temperature are too high and do not correspond to the conditions normally encountered in practice. Several iterative tests have had to be performed in order to obtain a reasonable temperature drop. In particular it was found to be impossible to use less than three circuits for this case (case B). Therefore the configuration selected was that of three circuits, respectively 3, 4 and 4 rows deep (in the direction of air flow). The geometry, core dimensions and relevant operating conditions for both configurations are summarized in Table 6.

Two types of results deserve attention: global results summarized in Table 7 and detailed results presented in (Fig. 23) and (Fig. 24). Table 7 shows that when reducing the tube diameter in Case B, internal pressure losses (refrigerant side) increase significantly, a fact that

results in an important evaporation temperature glide. It can be observed that for the given conditions, while the base configuration of Case A results in a pressure loss of 58 kPa over a single circuit in excess of 90 m, the Case B configuration uses three circuits with the respective lengths of 45.12 m, 60.16 m, 60.16 m. The internal pressure loss in each of them is 66 kPa, corresponding to a temperature glide of 1.4 °C. These results have direct repercussions on the total capacity produced by each coil: the configuration of Case B gives a 19% increase in capacity over the base configuration (Case A), mainly due to better heat transfer across the coil. The first and second circuits perform well while the third circuit produces less than half the capacity of the first circuit, evaporating only 20% of the available CO_2. This is due to the more important temperature gradients between air and CO_2, available for the first rows, corresponding to air inlet.

		Case A (Base Case)	Case B
Internal/external diameter		d_i/d_o=9.525/12.7 mm	d_i/d_o=6.35/9.52 mm
Longitudinal and transversal tube pitch		P_l/P_t=28.03/31.75 mm	P_l/P_t=20.39/23.81 mm
Tubes number/total length (m)		48/90.24 m	88/165.44 m
		118 fins/m, fin thickness= 0.19 mm, Pass length =1.88 m	
Inlet conditions	Air	$Tair_{in}$=-24.0 °C, $Pair_{in}$=101.3 kPa, HR_{in}=0.5, $\dot{m}_{air} = 1.105 kg/s$	
	CO_2	Tco_{2in}=-30.0 °C, quality=X=0%	

Table 6. Geometrical data and operational conditions

		Case A (Base case)	Case B
CO_2	Total pressure drop per circuit (kPa)	58.0	66.3
	ΔT of refrigerant per circuit (C)	1.19	1.4
	CO_2 mass flow rate per circuit (g/s)	12.2	6.7 circuit n°1 6.7 circuit n°2 15.0 circuit n°3
	Outlet CO_2 quality (%)	100	100.0 circuit n°1 73.5 circuit n°2 20.0 circuit n°3
	Power (W)	3699.8	2032.4 circuit n°1 1488.6 circuit n°2 874.8 circuit n°3 4395.8 (total)
Air	Total pressure drop (Pa)	48.87	49.35
Mass (kG)	Tubes	44.67	58.50
	Fins	1.60	1.56
	Total Coil Mass (kG)	46.27	60.06

Table 7. Results of comparison

The effect of tube diameter can also be presented in colors by the distribution of air temperature in (Fig. 23) and (Fig. 24). It is important to point out that the -28 °C of air temperature at the exit of the coil in case A can be reached at the end of the eighth row in

case B. This means that the coil volume as well as the mass of material can be reduced by 27 % without affecting the evaporation capacity. It was previously shown that under the same operating conditions, using CO_2 as a refrigerant in coils having tube diameters of 3/8 inches incur a smaller internal pressure drop in comparison with other commonly used synthetic refrigerants such as R507A for the case of supermarkets. Taking these results into account allows the use of longer circuits (as in Case A), therefore reducing their number and simplifying the overall configuration for a given capacity. The tube diameter has a great impact on the capacity and pressure drop of CO_2. Advantage can be taken of CO_2 thermo physical properties by using more tubes with small diameter, arranged in an appropriate number of circuits such that it becomes possible to reduce both the size and the mass of the coil while maintaining or even improving the capacity.

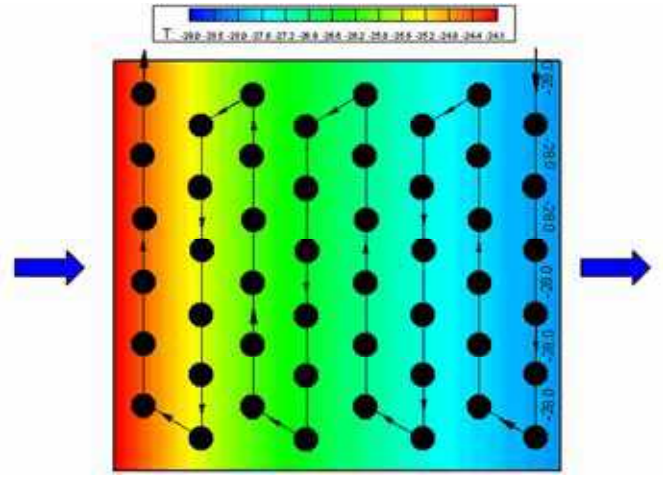

Fig. 23. Isotherms Case A (Base case)

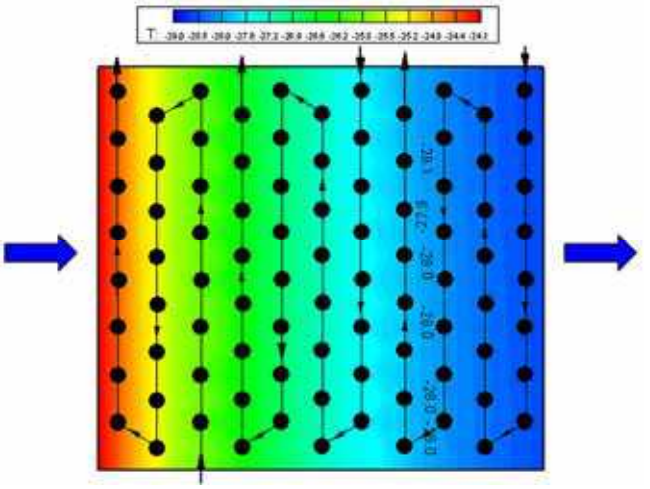

Fig. 24. Isotherms Case B

5. Conclusion

Finned tube heat exchangers are almost exclusively used as gas-to-liquid heat exchangers in a number of generic operations such as HVAC, dehumidification, refrigeration, freezing etc…, because they can achieve high heat transfer in reduced volume at a moderate cost. An improved coil design can considerably benefit the cycle efficiency, which is reflected in the coefficient of performance (COP). To this end, two different solution procedures were introduced in the modeling: the Forward Marching Technique (FMT) and the Iterative Solution for Whole System (ISWS). FMT solves the conservation equations one elementary control volume at a time before moving to the next while ISWS resolves simultaneously the conservation equations arranged in a matrix form for all the elements. Both procedures offer good flexibility for local simulations. The first was limited to dry operation and simple circuitry as a trade-off against relative simplicity while the second with its original indexing and parameterization method of flow directions, circuits and other relevant information offers extended capabilities for complex configurations and frosting conditions. The proposed models were validated against sets of data obtained on a dedicated refrigeration facility, and from the literature. Comparison of numerical predictions and experimental results were shown to be in very good agreement.

The tool was then successfully applied to predict coil performance under different practical conditions and simulation results were analysed. More particularly, it was shown that with this procedure, parameters of a three-dimensional coil could be represented by using a 1-dimensional approach, within reasonable limits of calculation accuracy, by tracking refrigerant and air flows inside tubes and across passes. The influence of non uniformities in air flow and the refrigerant local behavior could in this way be tackled. CO_2, a natural refrigerant was selected as the main fluid of study with which some other current refrigerants were compared. Its pressure drop in typical refrigeration conditions was shown to be very low in comparison to traditional refrigerants and resulting in very small temperature glides.

The effect of frost growth was studied in conjunction with the fin effect. This has shown that in general, frost initially enhanced heat transfer as long as the frost layer was sufficiently thin. Beyond this, the trend was changed with the least fins being more efficient. Large fin spacing delayed channel blockage and extended operation time.

The tool was also applied to study circuiting and its effects on coil operation and performance for different configurations of evaporation paths with CO_2 as the working fluid. The basic unit had only one circuit forming the whole coil and served as a reference. The other configurations had two circuits with different refrigerant paths but with the same total area and tube length. Comparison between these units has shown that circuiting affected performance and general coil operation. Internal pressure drop and corresponding temperature glides were greatly reduced, making it possible to use longer and fewer circuits with CO_2 as opposed to other refrigerants for similar refrigeration capacities. Combined effects of circuiting and tube diameters were then used to take advantage of the favourable thermo-physical characteristics of CO_2 in order to highlight the benefits in terms of size reductions. This exercise has demonstrated that by reducing the tube diameter and by increasing the number of circuits, it was possible to reduce both the size and the mass of the coil by at least 20% without affecting its capacity.

6. Acknowledgments

Funding for this work was mainly provided by the Canadian Government's Program on Energy Research and Development (PERD). The authors thank the Natural Sciences and

Engineering Research Council of Canada (NSERC) for the scholarship granted to the third author.

7. References

Aidoun Z. & Ouzzane M., 2005, Evaporation of Carbon Dioxide: A Comparative Study With Refrigerants R22 and R134A, *20th Canadian Congress of Applied Mechanics (CANCAM2005)*, May 30-June 2, Mc Gill, Montreal, Quebec, Canada.

Aidoun Z. & Ouzzane M., 2009, A Model Application to Study Circuiting and Operation in CO_2 Refrigeration Coils, *Applied Thermal Engineering*, Vol. 29, 2544-2553.

Aljuwayhel N.F., Reindl D.T., Klein S.A. & Nellis G.F., 2008, Comparison of parallel and counter-flow circuiting in an industrial evaporator under frosting conditions, *International Journal of Refrigeration*, 31: 98-106.

ASHRAE, 1993, *ASHRAE Handbook of Fundamentals*, SI Edition, chapter 6, pp.1-17, U.S.A.

ASHRAE, 2000, Methods of testing forced circulation air cooling and heating coils, *ASHRAE Standard* 33-2000, Atlanta, Georgia, U.S.A.

ASHRAE, 1987, Standard Methods for Laboratory Airflow Measurement, *ANSI/ASHRAE Standard* 41.2 (RA92), Atlanta, Georgia, U.S.A.

Bendaoud A., Ouzzane M., Aidoun Z. & Galanis N., Oct. 2010, A New Modeling Procedure for Circuit Design and Performance Prediction of Evaporator Coil Using CO_2 as Refrigerant, *Applied Energy*, Vol. 87, Issues 10, 2974-2983.

Bendaoud A., Ouzzane M., Aidoun Z. & Galanis N., July 2011, A Novel Approach to Study the Performance of Finned-Tube Heat Exchangers Under Frosting Conditions, *Journal of Applied Fluid Mechanics*, will be published in Vol. 4, Number 2, Issue 8 in July 2011.

Bensafi A., Borg S. & Parent D., 1997, CYRANO: A computational model for the detailed design of plate-fin-and-tube heat exchangers using pure and mixed refrigerants, *International Journal of Refrigeration*, 20(3): 218–28.

Byun J. S., Lee J. & Choi J. Y., 2007,Numerical analysis of evaporation performance in a finned-tube heat exchanger, *International Journal of Refrigeration*, 30: 812-820.

Chuah Y.K., Hung C.C.& Tseng P.C., 1998, Experiments on the dehumidification performance of a finned tube heat exchanger, *HVAC&R Research*, 4(2): 167-178.

Corberan J.M. & Melon M.G., 1998, A modeling of plate finned tube evaporators and condensers working with R134A, *International Journal of Refrigeration*, 21(4): 273–83.

Domanski P.A., 1989, EVSIM- An evaporator simulation model accounting for refrigerant with and one-dimensional air distribution, NIST report, *NISTIR*, 89-4133.

Domanski, P.A., 1991, Simulation of an evaporator with non-uniform one-dimensional air distribution, *ASHRAE Transaction*, 97 (1), 793-802.

Drew T.B., Koo E.C. & Mc Adams W.H., 1932, The friction factors for clean round pipes, *Trans. AIChE*, Vol. 28-56.

Ellison, P.R., F.A. Crewick, S.K. Ficher & W.L. Jackson, 1981, A computer model for air-cooled refrigerant condenser with specified refrigerant circuiting, *ASHRAE Transaction*, 1106-1124.

Geary D.F., 1975, Return bend pressure drop in refrigeration systems, *ASHRAE Transactions*, Vol. 81, No. 1, pp. 250-264.

Guo X.M., Chen Y.G., Wang W.H. & Chen C.Z., 2008, Experimental study on frost growth and dynamic performance of air source heat pump system, *Applied Thermal Engineering*, 28: 2267-2278.

Hwang Y., Kim B.H. & Radermacher R., Nov. 1997, Boiling heat transfer correlation for carbon dioxide, *IIR international conference*, Heat Transfer Issues in Natural Refrigeration.

Incropera F.P. & DeWitt D.P., 2002, *Fundamentals of heat and mass transfer*, John Wiley and Sons, 5th edition, NY.

Jones & Parker J.D., 1975, Frost formation with varying environmental parameters, *Journal of Heat Transfer*,Vol.97, pp. 255–259.

Jiang H., Aute V. & Radermacher R., 2006, Coil Designer: A general-purpose simulation and design tool for air-to-refrigerant heat exchangers, *International Journal of Refrigeration*, 601–610.

Kakaç S. & Liu H., 1998, *Heat exchangers, Selection, Rating and Thermal Design*, CRC Press LLC.

Kays W. M. & London A. L., 1984, *Compact Heat Exchangers*, 3rd edition, New York, McGraw-Hill.

Kondepudi S.N. & O'Neal D.L., 1993a, Performance of finned-tube heat exchangers under frosting conditions: I. Simulation model, *International Journal of Refrigeration*, Vol. 16, No. 3, pp. 175-180.

Kondepudi S. N. & O'Neal D. L., 1993b, Performance of Finned-Tube Heat Exchangers Under Frosting Conditions II : Comparison of Experimental Data with Model, *International Journal of Refrigeration*, Vol.16,No 3, 181-184.

Kuo M.C., Ma H. K., Chen S. L. & Wang C.C., 2006, An algorithm for simulation of the performance of air-cooled heat exchanger applications subject to the influence of complex circuitry, *Applied Thermal Engineering*, 26: 1- 9.

Lee K.S., Kim W.S. & Lee T.H., 1997, A one-dimensional model for frost formation on a cold flat surface, *International Journal of Heat Mass Transfer*, Vol. 40 No.18, pp. 4359-4365.

Liang S.Y., Liu M., Wong T. N. & Nathan G. K., 1999, Analytical study of evaporator coil in humid environment, *Applied Thermal Engineering*, 19: 1129-1145.

Liang, S.Y., Wong, T.N. & Nathan, G.K., 2001, Numerical and experimental studies of refrigerant circuitry of evaporator coils, *International Journal of Refrigeration*, 24, pp.823-833.

Liang S. Y., Wong T. N. & Nathan G. K., 2000, Study on refrigerant circuitry of condenser coils with exergy destruction analysis, *Applied Thermal Engineering*, 20: 559-577.

Liu J., Wei W., Ding G., Zhang C., Fukaya M., Wang K. & Inagaki T., 2004, A general steady state mathematical model for fin-and-tube heat exchanger based on graph theory, *International Journal of Refrigeration*, 27: 965- 973.

NIST, July 1998, *Thermodynamic and Transport Properties of Refrigerant Mixtures-REFPROP*, Version 6.01, U.S. Department of Commerce, Technology Administration.

Ogawa K., Tanaka N. & Takeshita M., 1993, Performance improvement of plate-fin-and-tube heat exchangers under frosting conditions, *ASHRAE Transactions*, CH-93-2-4: 762-771.

Ouzzane M. & Aidoun Z., 2008, A Numerical Study of a Wavy Fin and Tube CO_2 Evaporator Coil, *Heat Transfer Engineering*, Vol. 29, 12, 1008-1017.

Ouzzane M. & Aidoun Z., 2004, A numerical procedure for the design and the analysis of plate finned evaporator coils using CO_2 as refrigerant, *CSME Forum (The Canadian Society for the Mechanical Engineering)*, June1-4, 2004, London, Ontario, Canada.

Ouzzane M. & Aidoun Z., 2007, A Study of The Effect of Recirculation On An Air-CO_2 Evaporator Coil in A Secondary Loop of A Refrigeration System; *Heat SET 2007 Conference*, Chambery, 18-20 April, pp. 877-884, France.

Ouzzane M. & Aidoun Z., 2008, A Study of a Wavy Fin and Tube CO_2 Evaporator Coil for a Secondary Loop in a Low Temperature Refrigeration System, *International Conference, Design and Operation of Environmentally Friendly Refrigeration and AC Systems*, October 15-17, Poznan, Poland.

Rich D.G., 1973, The effect of fin spacing on the heat transfer and friction performance of multi-row, plate fin-and-tube heat exchangers, *ASHRAE Transactions*, 79 (2): 137-145.

Rich D.G., 1975, The effect of number of tube row on heat transfer performance of smooth plate fin-and-tube heat exchangers, ASHRAE Transactions, 81 (1): 307-317.

Rohsenow, W.M., Hartnett, J.P. and Cho and Y.I., 1998, *Handbook of Heat Transfer*, Third Edition, Mc Graw Hill, New York, pp. 17.89-17.97.

Seker D., Karatas H. & Egrican N., 2004a, Frost formation on fin-and-tube heat exchangers. Part I-Modeling of frost formation on fin-and-tube heat exchangers, *International Journal of Refrigeration*, 27(4): 367-374.

Seker D., Karatas H. & Egrican N., 2004b, Frost formation on fin-and-tube heat exchangers. Part II-Experimental investigation of frost formation on fin- and tube heat exchangers, *International Journal of Refrigeration*, 27(4): 375-377.

Singh V., Aute V. & Radermacher R., 2008, Numerical approach for modeling air-to-refrigerant fin-and-tube heat exchanger with tube-to-tube heat transfer, *International Journal of Refrigeration*, 31: 1414-1425.

Singh V., Aute V. & Radermacher R., 2009, A heat exchanger model for air-to- refrigerant fin-and-tube heat exchanger with arbitrary fin sheet, *International Journal of Refrigeration*, 32: 1724-1735.

Shokouhmand H., Esmaili E., Veshkini A. & Sarabi Y., Jan. 2009, Modeling for predicting frost behaviour of a fin-tube heat exchanger with thermal contact resistance, *ASHRAE Transactions*, pp. 538-551.

Stoecker W.F., 1957, How frost formation on coils effects refrigeration systems, Refrigeration Engineering, 42.

Stoecker W.F., 1960, Frost formation on refrigeration coils, *ASHRAE Trans.*, 66:91.

Vardhan A., Dhar P.L., 1998, A new procedure for performance prediction of air conditioning coils, *International Journal of Refrigeration*, 21(1): 77–83.

Wang C. C., Chang Y. J., Hsieh Y. C. & Lin Y. T., 1996, Sensible heat and friction characteristics of plate-fin-and-tube heat exchangers having plain fins, *International Journal of Refrigeration*, 19(4): 223-230.

Wang C.C., Hsieh Y. C. & Lin Y. T., 1997, Performance of plate finned tube heat exchangers under dehumidifying conditions, *Journal of Heat Transfer*, 11(9): 109-117.

Wang, C.C., Hwang, Y.M. & Lin, Y.T., 2002, Empirical correlations for heat transfer and flow friction characteristics of herringbone wavy fin-and-tube heat exchangers, *International Journal of Refrigeration*, Vol. 25, pp.673- 680.

Yang D., Lee K. & Song S., 2006a, Modeling for predicting frosting behaviour of a fin-tube heat exchanger, International *Journal of Heat and Mass Transfer*, 49 (7-8): 1472-1479.

Yang D., Lee K. & Song S., 2006b, Fin spacing optimization of a fin-tube heat exchanger under frosting conditions, *International Journal of Heat and Mass Transfer*, 49 (15-16): 2619-2625.

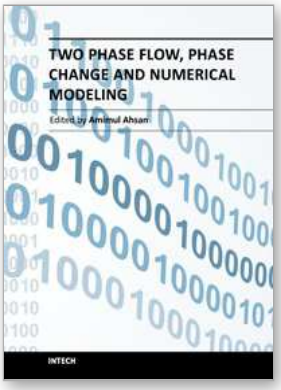

Two Phase Flow, Phase Change and Numerical Modeling

Edited by Dr. Amimul Ahsan

ISBN 978-953-307-584-6
Hard cover, 584 pages
Publisher InTech
Published online 26, September, 2011
Published in print edition September, 2011

The heat transfer and analysis on laser beam, evaporator coils, shell-and-tube condenser, two phase flow, nanofluids, complex fluids, and on phase change are significant issues in a design of wide range of industrial processes and devices. This book includes 25 advanced and revised contributions, and it covers mainly (1) numerical modeling of heat transfer, (2) two phase flow, (3) nanofluids, and (4) phase change. The first section introduces numerical modeling of heat transfer on particles in binary gas-solid fluidization bed, solidification phenomena, thermal approaches to laser damage, and temperature and velocity distribution. The second section covers density wave instability phenomena, gas and spray-water quenching, spray cooling, wettability effect, liquid film thickness, and thermosyphon loop. The third section includes nanofluids for heat transfer, nanofluids in minichannels, potential and engineering strategies on nanofluids, and heat transfer at nanoscale. The forth section presents time-dependent melting and deformation processes of phase change material (PCM), thermal energy storage tanks using PCM, phase change in deep CO2 injector, and thermal storage device of solar hot water system. The advanced idea and information described here will be fruitful for the readers to find a sustainable solution in an industrialized society.

How to reference

In order to correctly reference this scholarly work, feel free to copy and paste the following:

Zine Aidoun, Mohamed Ouzzane and Adlane Bendaoud (2011). Numerical Modeling and Experimentation on Evaporator Coils for Refrigeration in Dry and Frosting Operational Conditions, Two Phase Flow, Phase Change and Numerical Modeling, Dr. Amimul Ahsan (Ed.), ISBN: 978-953-307-584-6, InTech, Available from: http://www.intechopen.com/books/two-phase-flow-phase-change-and-numerical-modeling/numerical-modeling-and-experimentation-on-evaporator-coils-for-refrigeration-in-dry-and-frosting-ope

INTECH
open science | open minds

InTech Europe
University Campus STeP Ri
Slavka Krautzeka 83/A
51000 Rijeka, Croatia
Phone: +385 (51) 770 447
Fax: +385 (51) 686 166
www.intechopen.com

InTech China
Unit 405, Office Block, Hotel Equatorial Shanghai
No.65, Yan An Road (West), Shanghai, 200040, China
中国上海市延安西路65号上海国际贵都大饭店办公楼405单元
Phone: +86-21-62489820
Fax: +86-21-62489821